

# Tips for implementing multigrid methods on domains containing holes

Scott H. Hawley and Richard A. Matzner

Center for Relativity, University of Texas at Austin, Austin, Texas 78712 USA

E-mail: shawley@physics.utexas.edu, matzner@physics.utexas.edu

PACS numbers: 0.420C, 0.425, 0.425Dm

**Abstract.** As part of our development of a computer code to perform 3D ‘constrained evolution’ of Einstein’s equations in 3+1 form, we discuss issues regarding the efficient solution of elliptic equations on domains containing holes (i.e., excised regions), via the multigrid method. We consider as a test case the Poisson equation with a nonlinear term added, as a means of illustrating the principles involved, and move to a “real world” 3-dimensional problem which is the solution of the conformally flat Hamiltonian constraint with Dirichlet and Robin boundary conditions. Using our vertex-centered multigrid code, we demonstrate globally second-order-accurate solutions of elliptic equations over domains containing holes, in two and three spatial dimensions. Keys to the success of this method are the choice of the restriction operator near the holes and definition of the location of the inner boundary. In some cases (e.g. two holes in two dimensions), more and more smoothing may be required as the mesh spacing decreases to zero; however for the resolutions currently of interest to many numerical relativists, it is feasible to maintain second order convergence by concentrating smoothing (spatially) where it is needed most. This paper, and our publicly available source code, are intended to serve as semi-pedagogical guides for those who may wish to implement similar schemes.

## 1. Introduction

Solving Einstein’s equation in 3+1 form [1, 2] requires that a set of elliptic (or quasi-elliptic) constraint equations be satisfied at all times. The Bianchi identities ensure that, given a set of initial data which analytically satisfy the constraints, the subsequent analytically evolved variables will also satisfy the constraints. In numerical solutions of Einstein’s equations, however, the constraints are not preserved exactly. Thus errors will arise as the simulation proceeds, and the extent to which the numerical solutions actually reflect the true solutions of the analytic equations is still an open area of research (e.g., [3, 4, 5, 6, 7]). Apart from the issue of the accuracy of the solutions obtained, there is also the problem of numerical (in)stability, which seems to be related to the lack of preservation of the constraints.

It has been observed for lower-dimensional computational relativity simulations [8, 9, 10] that the use of “constrained evolution” schemes, in which the constraint equations are satisfied (to some fixed accuracy) at all timesteps, can offer better stability behavior. Such schemes have not yet received adequate attention in 3D simulations simply because of the costly nature of solving the constraints at every

timestep. We are among a set of researchers (e.g., [11, 12, 13]) interested in exploring the benefits of constrained evolution for 3D applications.

Our desire to solve the constraints at each timestep motivates us to develop a *fast* elliptic solver with which to enforce the constraints, and we turn our attention to one of the most popular methods currently in use: the multigrid method [14]. The multigrid method is particularly attractive because it is an optimal method, i.e. it requires only  $O(N)$  operations, where  $N$  is the number of unknowns. Furthermore, the multigrid method is not especially difficult to implement. (Although multidomain pseudospectral collocation methods [15, 16] also offer very efficient solutions of elliptic problems, we focus on multigrid because of the relative ease with which one can develop a multigrid code. It is not our intent in this paper to present a comparison between multigrid methods and other numerical methods.) In the course of developing our own implementation of the multigrid method containing holes (i.e., excised regions), it came to our attention that some researchers consider it impossible, or at least infeasible in practice, to obtain generic results which have everywhere the same order of accuracy as the finite difference scheme employed, for domains containing holes, particularly in three dimensions. (Specifically, that, using second-order-accurate difference stencils, one could not generically obtain second-order-accurate multigrid solutions if part of the domain was excised.)

Since we expect to use exact, analytic data as an inner Dirichlet boundary condition (at the surface of the hole), we believe it is not necessary to employ ‘sophisticated’ schemes such as deferred correction [17], which can be used to achieve higher order accuracy for various boundary conditions. We are already aware that one can fairly easily obtain second order convergence using square (in 2D) or cubical (in 3D) excision regions in which the physical domain of the hole is the same on all multigrid levels. However, we wish to apply our multigrid code in situations where the shapes of the holes are more general (e.g., spherical holes). Thus we are motivated to find a simple, robust method to handle the physical situations of interest to us.

If the multigrid solver is to be used to provide initial data for a numerical evolution code, the error of the initial solution need only be below the truncation error of the finite difference scheme used for evolution [18]. Thus our pursuit of specifically *second order* convergence for the multigrid scheme might be regarded as unnecessary. Our motivation is partly to develop a simple algorithm which nevertheless offers fast (better than first order) convergence, and partly because, given our exact Dirichlet conditions for the inner boundary, we simply expect that it should not be difficult to obtain second order convergence from the multigrid solver.

Although it is likely the case that some of the techniques presented here are known to some specialists, we believe it is worthwhile to popularize the straightforward methods we have used.

If we were applying a numerical method to a new physical system, we would want to provide a full discussion of mathematical foundations, for issues such as existence and uniqueness of the solutions. Since the use of finite difference techniques to solve the constraint equations is by now a standard activity in relativity, and the properties of the constraint equations are well known (for the Euclidean, constant-mean-curvature background and for the signs of the solutions we use in this paper [19, 20, 21]), we will focus our attention on the benefits of our multigrid implementation: second order accuracy near the hole via a simple method, and the efficiency improvements afforded by concentrating smoothing near the hole and performing more smoothing sweeps during the pre-Coarse-Grid-Correction (CGC) phase than during the post-

CGC phase. The validity of our results will be established by demonstrating second order convergence to known exact solutions as well as second order behaviour in the truncation error.

The organization of this paper is as follows: We begin with an overview of the multigrid method. We then discuss some results obtained in two dimensions, which we then extend toward a more difficult equation in three dimensions, eventually demonstrating the method by solving the Hamiltonian constraint equation for a black hole (with additional matter) on a Euclidean background. Finally we share some ideas for more general applications, and we end with a summary of the main five ‘tips’ we have for others wishing to implement multigrid methods on domains with holes.

## 2. Overview of Multigrid

The multigrid method, first introduced by Brandt [14], has received considerable attention in the literature, and is the subject of numerous articles, conferences, reviews and books (e.g., [22, 23, 24, 25, 26, 27]). However, its application on domains with holes — or on domains with “irregular boundaries” in general — has received only modest attention. The excellent works of Johansen and Colella [28] and Udaykumar et al. [29] for cell-centered multigrid are notable exceptions. The “BAM” code [30] is a notable introduction of the multigrid method in numerical relativity, and even features the ability to handle domains with multiples holes. (It does not employ the advances we describe in this paper, notably our method of obtaining second order accuracy near the hole.) Despite this significant result, multigrid methods in numerical relativity remain as tools of only a few specialists. We thus thought it worthwhile to share our experiences and methods with *vertex-centered* multigrid with the numerical relativity community.

A simple algorithm to solve discretized elliptic equations is Gauss-Seidel relaxation [31]. This method works very poorly at high resolutions because it fails to operate efficiently on long-wavelength components of the error. However, it is extremely effective at eliminating short-wavelength components of the error, or in other words, at “smoothing” the error (i.e., the residual, see below). The multigrid scheme is essentially a clever means of eliminating successive wavelength-components of the error via the use of relaxation at multiple spatial scales.

Here we give a very brief overview of the multigrid method, following the notes by Choptuik [32]. (Introductions to multigrid applications in numerical relativity are also found in Choptuik and Unruh [33] and Brandt [34].) We want to solve a continuum differential equation  $\mathcal{L}u = f$ , where  $\mathcal{L}$  is a differential operator,  $f$  is some right hand side, and  $u$  is the solution we wish to obtain. We discretize this differential equation into a *difference* equation on some grid (or lattice) with uniform spacing  $h$ :

$$\mathcal{L}^h u^h = f^h, \quad (1)$$

where  $u^h$  is the *exact* solution of this discrete equation, and  $\lim_{h \rightarrow 0} u^h = u$ . Rather than attempting to solve (1) directly via the costly operation of matrix inversion, we apply an iterative solution method. At any step in our iteration, we will have only an approximate solution  $\tilde{u}^h \simeq u^h$ , such that

$$\mathcal{L}^h \tilde{u}^h - f^h = \tilde{r}^h, \quad (2)$$

where  $\tilde{r}^h$  is some small quantity called the *residual*. The variables  $u^h$  and  $\tilde{u}^h$  are related by

$$u^h = \tilde{u}^h + v^h, \quad (3)$$

where  $v^h$  is some *correction* term. In this iterative algorithm, we start with some guess  $\tilde{u}_{\text{old}}^h$  and try to bring it closer to  $u^h$  by applying some (approximate) correction:

$$\tilde{u}_{\text{new}}^h := \tilde{u}_{\text{old}}^h + \tilde{v}^h \quad (4)$$

The remainder of the scheme involves making a choice of what to use for  $\tilde{v}^h$ . A simple choice, called the Linear Correction Scheme (LCS), can be used for linear operators  $\mathcal{L}^h$ . This method can then be extended to work with nonlinear operators via the Full Approximation Storage (FAS) method, below.

### 2.1. Linear Correction Scheme (LCS)

For linear  $\mathcal{L}$ , we begin by substituting (3) into (1):

$$\mathcal{L}^h(\tilde{u}^h + v^h) = f^h. \quad (5)$$

Then we use the linearity of  $\mathcal{L}$ :

$$\mathcal{L}^h \tilde{u}^h + \mathcal{L}^h v^h = f^h, \quad (6)$$

$$\begin{aligned} \mathcal{L}^h v^h &= f^h - \mathcal{L}^h \tilde{u}^h \\ &= -\tilde{r}^h. \end{aligned} \quad (7)$$

Consider a coarser-grid version of (7), in which we use a mesh spacing of  $2h$ :

$$\mathcal{L}^{2h} v^{2h} = -\tilde{r}^{2h}. \quad (8)$$

Now we come to one of the ‘tricks’ of the multigrid method: Instead of the coarser residual in equation (8), use

$$\tilde{r}^{2h} = I_h^{2h} \tilde{r}^h, \quad (9)$$

where  $I_h^{2h}$  is a *restriction* operator, which maps values from the fine grid to the coarse grid via some weighted averaging operation. So then we have

$$\mathcal{L}^{2h} \tilde{v}^{2h} = -I_h^{2h} \tilde{r}^h. \quad (10)$$

(Note the tilde on  $\tilde{v}^{2h}$ , denoting that this is not the exact  $v^{2h}$ , because we use a residual restricted from the fine grid.) Equation (10) can be solved “exactly” for  $\tilde{v}^{2h}$  because this is inexpensive to do on the coarse grid.

A second ‘trick’ is that, for our correction term  $\tilde{v}^h$  in our numerical update scheme (4), we do not directly solve equation (7), but instead we use  $\tilde{v}^h$  approximated from the coarser ( $2h$ ) correction  $\tilde{v}^{2h}$ :

$$\tilde{v}^h = I_{2h}^h \tilde{v}^{2h}, \quad (11)$$

where  $I_{2h}^h$  is an interpolation or *prolongation* operator, which maps values from the coarse grid to the fine grid via some interpolation operation. Thus we use  $\tilde{v}^{2h}$  as a *coarse grid correction* (CGC) to  $\tilde{u}^h$ :

$$\tilde{u}_{\text{new}}^h := \tilde{u}_{\text{old}}^h + I_{2h}^h \tilde{v}^{2h}. \quad (12)$$

In performing the restriction  $\tilde{r}^{2h} = I_h^{2h} \tilde{r}^h$ , we are assuming that  $\tilde{r}^h$  is sufficiently smooth to be sensibly represented on the coarse grid (e.g., without aliasing effects). This implies that  $\tilde{u}^h$  also needs to be smooth for this restriction to produce meaningful results. Therefore, before each restriction operation, we apply a series of “smoothing sweeps” to  $\tilde{u}^h$  in an effort to smooth the residual  $\tilde{r}^h$ , using the efficient smoothing algorithm of Gauss-Seidel relaxation.

## 2.2. Full Approximation Storage (FAS) method

For nonlinear operators  $\mathcal{L}^h$ , we must modify the algorithm outlined above. Our implementation relies on the so-called “alternative” description of the FAS algorithm, which involves a notion of the truncation error  $\tau^{2h}$ , defined on the coarse grid by

$$\tau^{2h} \equiv \mathcal{L}^{2h}u - f^{2h}, \quad (13)$$

where  $u$  is the exact solution to the continuum equation. The function  $\tau^{2h}$  can be regarded as a correction term which makes the finite difference equation produce the continuum solution:

$$\mathcal{L}^{2h}u = f^{2h} + \tau^{2h}. \quad (14)$$

For general problems, the continuum solution  $u$  and truncation error  $\tau^{2h}$  may not be available, however we may use an approximation to  $\tau^{2h}$  which is the *relative* truncation error between the coarse and fine grids,  $\tau_h^{2h}$ , given by

$$\tau_h^{2h} \equiv \mathcal{L}^{2h}I_h^{2h}\tilde{u}^h - I_h^{2h}\mathcal{L}^h\tilde{u}^h. \quad (15)$$

Using this in (14) gives

$$\mathcal{L}^{2h}u^{2h} \simeq f^{2h} + \tau_h^{2h}, \quad (16)$$

and it is this equation which we solve on the coarse grid.

To obtain the CGC to a fine grid solution, we substitute (15) into (16), obtaining

$$\mathcal{L}^{2h}u^{2h} - \mathcal{L}^{2h}I_h^{2h}\tilde{u}^h = I_h^{2h}(f^h - \mathcal{L}^h\tilde{u}^h), \quad (17)$$

where the term  $I_h^{2h}f^h$  on the right is introduced for  $f^{2h}$ , in analogy with equation (8). By analogy to (10) in the LCS scheme, the term we should use for the CGC is (the part on the left hand side of the previous equation, without the  $\mathcal{L}$ 's):

$$\tilde{v}^{2h} = u^{2h} - I_h^{2h}\tilde{u}^h. \quad (18)$$

Thus we arrive an update scheme of

$$\tilde{u}_{\text{new}}^h := \tilde{u}_{\text{old}}^h + I_{2h}^h(u^{2h} - I_h^{2h}\tilde{u}^h). \quad (19)$$

Note that  $u^{2h}$  is the exact solution to (16), and can be obtained with little effort due to the low resolution on the coarse grid. (If there are more than two multigrid levels involved in the solution, then  $u^{2h}$  should be the best approximation  $\tilde{u}^{2h}$  obtained on the coarser grid.)

## 2.3. V-Cycles and the Full Multigrid Algorithm

Instead of only using two grids as described above, one could find the coarse grid correction (CGC) to a fine-grid-problem by solving for a CGC from an even coarser grid, i.e., obtain  $\tilde{u}^{2h} \simeq u^{2h}$  by finding  $u^{4h}$  (in which case the corresponding right hand side is  $f^{4h} + \tau_{2h}^{4h}$ , where  $f^{4h} \equiv I_{2h}^{4h}[f^{2h} + \tau_h^{2h}]$ ). One can imagine a hierarchy of multiple such grids, in which coarser grids provide CGCs for finer grids. The solution algorithm will then take the form of a *V-cycle*, in which we start with an initial guess on the fine grid, at multigrid level  $l_{\text{max}}$ . Then we perform some number of smoothing sweeps and restrict the data to a coarser grid. We continue smoothing and restricting to coarser grids until we arrive at a grid coarse enough to solve the coarse grid equation (16) ‘exactly’ (i.e., to machine precision), at minimal computational cost. This coarsest grid is at level  $l_{\text{min}}$ . We then prolongate this solution to finer grids by performing a

series of coarse-grid corrections, with perhaps additional smoothing operations being performed before moving to each finer grid.

In addition, before starting a V-cycle from the finest grid, we can use an initial guess obtained from a prior solution at a coarser resolution. Doing this for each grid level results in the *Full Multigrid Algorithm* (FMA). We outline the FMA as follows, (using a notation where superscripts refer to multigrid levels, with  $l_{\min}$  the coarsest level, and  $l_{\max}$  the finest):

```

 $u^{l_{\min}} = u_0$  // Initial guess, e.g.  $u_0 = 0$ 
// or  $u_0 = 1$ 

Solve  $L^{l_{\min}} u^{l_{\min}} = f^{l_{\min}}$  ‘exactly’
do  $l = l_{\min} + 1$  to  $l_{\max}$ 
   $u^l = I_{l-1}^l u^{l-1}$  // Initial guess for fine grid
  // Begin V-cycle

  do  $m = l$  to  $l_{\min} + 1$ 
    Smooth (solve via Gauss-Seidel) at level  $m$  // Pre-CGC smooths
     $f^{m-1} = I_{m-1}^m f^m + \tau_m^{m-1}$  // Restrict to coarser grid
     $\tilde{u}^{m-1} = I_{m-1}^m \tilde{u}^m$  // Restrict to coarser grid
  end do

  Solve  $L^{l_{\min}} u^{l_{\min}} = f^{l_{\min}}$  ‘exactly’ // Solve on coarsest grid

  do  $m = l_{\min} + 1$  to  $l_{\max}$ 
     $u^l := u^l + I_{m-1}^m (u^{m-1} - I_m^{m-1} u^m)$  // Apply CGC
    Smooth at level  $m - 1$  // Post-CGC smooths
  end do

  // End V-cycle
end do // End FMA

```

Thus we see that on all grids except the coarsest grid, we only smooth the error, and we solve the difference equation exactly only on the coarsest grid.

### 3. Solution of a Nonlinear Poisson Equation

Since we are interested in ultimately solving for the constraint equations in general relativity, we consider the Hamiltonian constraint in a conformally flat background geometry. This yields the the Poisson equation with a pair of nonlinear terms added:

$$\nabla^2 u(x, y, z) - K^2 u^5(x, y, z) + \frac{A^2}{u^7(x, y, z)} = f(x, y, z), \quad (20)$$

where  $\nabla^2$  is the usual Laplacian in Euclidean space.  $K^2$  and  $A^2$  are arbitrary positive real constants related to the rate of expansion for the 3-space for which is (20) is the constraint equation.  $f(x, y, z)$  is related to the energy density in the 3-space, and can be chosen such that the resulting  $u(x, y, z)$  has some known (exact) form by which we can check our numerical results.

Rather than begin with this somewhat complicated equation, we begin by solving a slightly simpler-looking equation in two and three dimensions, in which the nonlinearity is of a quadratic form, as in

$$\nabla^2 u(x, y, z) + \sigma u^2(x, y, z) = f(x, y, z), \quad (21)$$

where  $\sigma (\in \mathbb{R})$  is some tunable parameter which we typically set to  $\pm 1$  (although there are good reasons to prefer  $-1$  over  $+1$ ; see footnote regarding smoothing operations, on the next page). We chose this equation not because of any particular physical relevance, but simply because it was the equation used in the version of Choptuik's 2D multigrid code [35], with which we had prior experience.

Before proceeding to 3D calculations, we will describe our implementation for solving a 2D version of (21). Due to memory limitations (and array-indexing limitations in many Fortran compilers), we can run our (non-parallel) 3D code only at much lower resolutions than we are able to achieve with the 2D code. Since some of the interesting features in the convergence studies appear only at very high resolutions in our 2D results, we first present our 2D scheme and the results yielded by it.

### 3.1. Two dimensions

Our starting point is a 2D FAS multigrid solver by Choptuik [35], which solves the equation

$$\frac{\partial^2}{\partial x^2} u(x, y) + \frac{\partial^2}{\partial y^2} u(x, y) + \sigma u^2(x, y) = f(x, y), \quad (22)$$

on a domain  $\Omega$  with coordinate ranges  $[0, 0]$  to  $[1, 1]$ , and subject to Dirichlet conditions at the outer boundary:  $u(x, y)|_{\partial\Omega_O} = \text{const.}$ , and we choose this constant to be zero. The function  $f(x, y)$  is chosen such that the solution is

$$u(x, y) = \sin(\pi l_x x) \sin(\pi l_y y), \quad (23)$$

where  $l_x$  and  $l_y$  are integers (which we set to unity for the cases presented in this paper). We also choose  $\sigma = 1$ . Choptuik's form assumed a domain without holes, but we extend this to configurations with holes, and on these inner boundaries we also apply Dirichlet conditions, the values for which are discussed below.

The code uses a hierarchy of so-called "vertex centered" grids. Each grid at multigrid level  $l$  is a square lattice having  $2^l + 1$  grid points along each edge. The grids have uniform spacing  $h_l = 2^{-l}$  in both  $x$  and  $y$  directions, and the grid points are denoted with indices  $i$  and  $j$  in the  $x$  and  $y$  directions, respectively, e.g.,  $u(ih_l, jh_l) \simeq \tilde{u}_{i,j}^h$ .

To Choptuik's original code, we added added features needed to handle the excision region. We also performed a few minor optimizations. At each grid point, we also store an integer code which denotes whether the point is a boundary point, an excised point, or an interior (or *active*) point. The set of all excised points is known as the *excision mask* or *mask*, and for the cases considered in this paper, we define the mask to be those points which are a distance  $r \leq r_{\text{mask}}$  from the center of the grid, where  $r_{\text{mask}}$  is some value of our own choosing. The outermost points of the mask are where the inner boundary conditions are applied; we refer to these points as "inner boundary points." In addition to the single-hole case, we will consider the case of two holes, for which the excision regions will be points within the radius  $r_{\text{mask}}$  from the center of each hole.

### Boundary Conditions

We use Dirichlet boundary conditions at both the inner boundary (edge of the hole) and the outer boundary, and apply them on all grid levels. At the outer boundary,

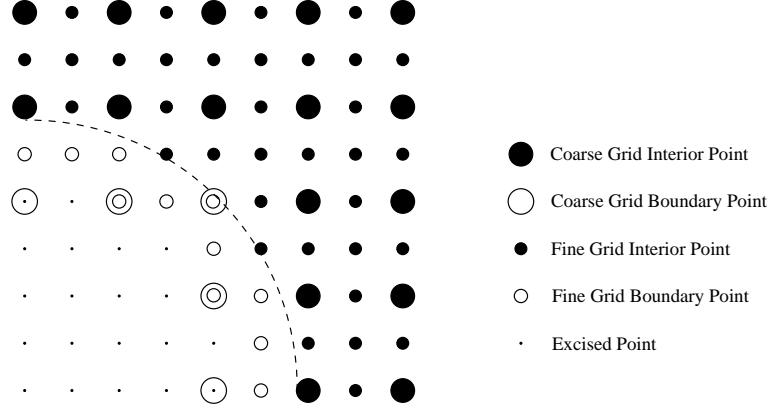


**Figure 1.** Example of how the inner boundary is defined, showing points on a coarse grid and a fine grid. Inner boundary points are those points which are immediately interior to a circle of radius  $r_{\max}$ . The large filled circles show normal interior grid points (i.e., non-excised, non-boundary points) on the coarse grid, and the large open circles show boundary points on the coarse grid. The small filled and open circles show fine grid interior points and boundary points, respectively. The small dots show excised points on the fine and/or coarse grids, as appropriate. (Only one quadrant of a full domain is shown in this picture for purposes of clarity, but our simulations are usually performed with the circle being centered on the grid.)

we simply set  $\tilde{u}^h = 0$ . At the inner boundary, we use the values of the exact solution, i.e., we set  $\tilde{u}^h = u(x, y)$ .

The inner boundary is given by the outer edge of the points comprising the excision mask; an example is shown in Figure 1. Thus, in some sense these boundary points are not truly “excised” since they have data on them. This has the consequence that the “size” of the excision region (i.e., the area of the convex hull of the data points comprising the mask) on finer grids is always equal to or greater than the size of the excision region on coarser grids. This choice of the inner boundary, as being those points just inside some level surface instead of just outside it, is somewhat at variance from other excision schemes used in numerical relativity (e.g., [36]). Our choice is not fundamentally based on physical or mathematical principles, and is thus somewhat arbitrary. However we find that this definition of the inner boundary appears to be a key to our results of second order convergence: if we instead define inner boundary points to be those just *beyond*  $r = r_{\max}$ , then we do not obtain second order convergence.

### Smoothing Operations

We use a typical “red-black” Gauss-Seidel Newton iteration to smooth the error on each grid, in which we loop over all ‘interior’ points (i.e. non-excised, non-boundary points) and apply the following two equations ‡

‡ We note an example of the care that must be taken in any solution of a discretized problem. Convergence of the solution may be impossible to achieve; this may signal significant analytical defects in the formulation. If  $\tilde{u} > 0$ , then  $\sigma = -1$  guarantees that the Jacobian  $2\sigma\tilde{u}_{i,j} - 4/h^2$  is nonzero (its inverse is nonsingular in Eq. (25)). Clearly, there are in principle situations with  $\sigma\tilde{u} > 0$  where the Jacobian can vanish. Further, because the equations we wish to solve are nonlinear, zeros



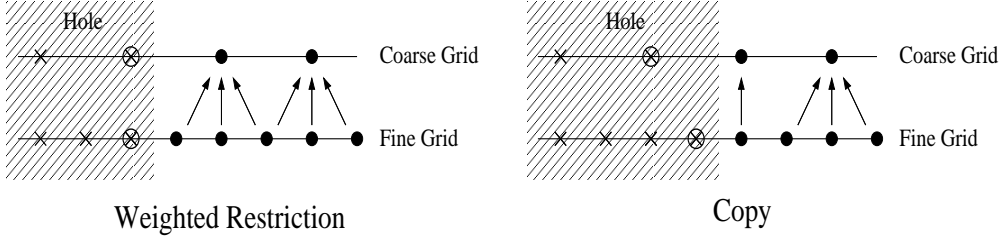


**Figure 2.** 1-D schematic of scheme for inner boundary and restriction scheme. The circles on the rightmost X's indicate that this is where the Dirichlet conditions are applied, i.e., there *are* data on these points for all quantities except  $\mathcal{L}^h \tilde{u}^h$  (which appears in (15)), which we do not compute on the boundary. One *could* use these points in weighted restriction even in the case shown in the right panel. However, we choose never to use these boundary data in weighted restriction, and instead do a simple “copy” operation.

$$r_{GS} = h^{-2} (\tilde{u}_{i+1,j} + \tilde{u}_{i-1,j} + \tilde{u}_{i,j+1} + \tilde{u}_{i,j-1} - 4\tilde{u}_{i,j}) + \sigma \tilde{u}_{i,j}^2 - f_{i,j} \quad (24)$$

$$\tilde{u}_{i,j}^{\text{new}} = \tilde{u}_{i,j}^{\text{old}} - \frac{r_{GS}}{2\sigma \tilde{u}_{i,j} - 4h^{-2}}. \quad (25)$$

### Restriction and Prolongation Operators

The restriction operator  $I_h^{2h}$  we use is the so-called “half-weighted” average on normal interior points, in which coarse grid values (indexed by  $I$  and  $J$  for clarity) are a weighted average of the fine grid values over a nearby region of the physical domain:

$$\tilde{u}_{I,J}^{2h} = I_h^{2h} \tilde{u}^h = \frac{1}{2} \tilde{u}_{i,j}^h + \frac{1}{8} [\tilde{u}_{i+1,j}^h + \tilde{u}_{i-1,j}^h + \tilde{u}_{i,j+1}^h + \tilde{u}_{i,j-1}^h], \quad (26)$$

where  $i = 2I - 1$  and  $j = 2J - 1$ . Along the outer boundary, we perform a simple copy operation,  $\tilde{u}_{I,J}^{2h} = \tilde{u}_{i,j}^h$ . We use (26) for all restriction operations on interior grid points with one exception: We only use weighted restriction if none of the fine grid points used in the restriction operator is on or inside the boundary of the excised region; otherwise we use a “simple injection” or “copy” operation. This is illustrated in Figure 2. In conjunction with our definition of the inner boundary location, this use of a “copy” operation near the inner boundary is the central insight for preserving second order accuracy near the excision region.

For the prolongation operator  $I_{2h}^h$ , we use simple bilinear interpolation.

#### 3.1.1. 2D Results

One of the first things we notice when graphing preliminary numerical solutions is that the solution error  $e \equiv u - \tilde{u}^h$  seems to be largest and “most in need of smoothing”

of the Jacobian depend on  $\tilde{u}$  and may occur at isolated spatial points. Further, because  $2\sigma \tilde{u}_{i,j}$  is similar on all grids, but  $-1/h^2$  is resolution dependent, this problem can appear differently on different multigrid levels. It may be that a more sophisticated solver could integrate through those singular points, but we do not address that question here. Notice that because  $\tilde{u}_{i,j}$  is near unity in the case of “sine” data given by Eq. (23), this problem does not arise for  $\sigma = 1$  for “sine” data. Similar comments apply, of course, in the 3D case of equation (21).

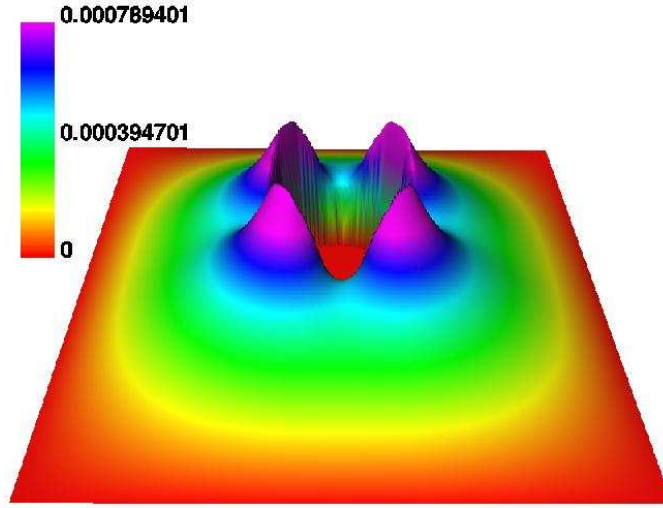


**Figure 3.** A plot of the solution error  $e = u - \tilde{u}^h$  for a system physical parameters  $\sigma = 1$  and  $l_x = l_y = 1$ . We use a central circular hole of radius  $r_{\text{mask}} = 0.129$ , where this number is chosen such that the excision masks on different grid levels do *not* match up with one another, i.e., to make the solution *harder* to obtain, in order to demonstrate the robustness of our multigrid scheme. We see that the error is largest and sharpest next to the circular hole in the center. Thus, concentrating our smoothing operations near the hole is likely to increase the efficiency of the solver. These data are obtained from a run with parameters  $L_{\text{max}} = 8$ ,  $L_{\text{min}} = 2$ , 1 V-cycle and 2 pre- and 2 post-CGC smoothing sweeps.

(i.e., having high-frequency components) in the immediate vicinity of the excision region, as shown in Figure 3.

Thus we may perform only a few smooths on the entire grid and apply extra smoothing runs in an “extra smoothing region” (ESR) around the excision region, such as that shown in the left panel of Figure 4. In our implementation, we choose the width of the ESR to be a number of grid points which is one less than the current multigrid level number (e.g., on a level 4 grid, the ESR has a width of 3 grid points), and we smooth over the ESR twice as often as over the rest of the domain. We can compare the results of using the extra smoothing region to the results of smoothing over the entire domain. Such a comparison is shown in the right panel of Figure 4. In our multigrid implementation, we always do twice as many smooths in the ESR as in the rest of the interior.

### Two Holes

One of our principal applications for the multigrid solver will be to solve the constraint equations for binary black hole spacetimes. Thus we do a check to make sure that, at least for the nonlinear Poisson equation, our general method properly handles domains with multiple holes. One such case is shown in Figure 5.

There is a contrast between the relative importance of pre-CGC smoothing versus post-CGC smoothing. Pre-CGC smoothing prepares the data in such a way that restriction will not produce aliasing errors, whereas post-CGC smoothing in large part corrects for errors brought in via the use of (linear) interpolation. It seems plausible

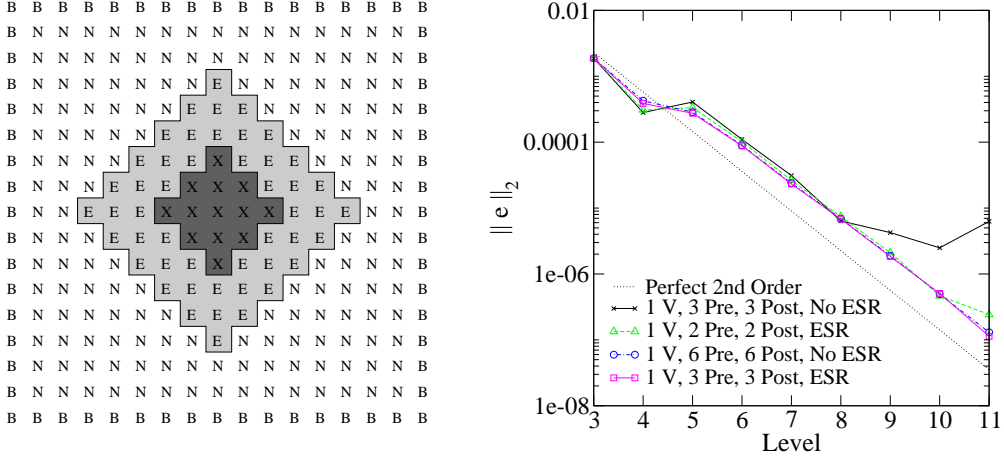


**Figure 4.** Left panel: Schematic of a level = 4 grid ( $2^{\text{level}} + 1$  grid points per side) showing excised points (X's), normal interior points (N's), boundary points (B's) and the Extra Smoothing Region (ESR, E's). In this case, the excision region has radius  $r_{\text{mask}} = 0.129$ . Right panel: Convergence behavior of Eqs. (22)-(25) with and without the use of the ESR. Here we show the L2 norm of the solution error  $e = u - \tilde{u}$ . We assign the width of ESR to be level  $- 1$  grid points on either side of the hole, and we smooth twice as often over the ESR as over the normal interior points. Since the error is concentrated near the hole, we see that using 2 pre- and post-CGC smooths with the ESR (i.e., using 4 smooths in the ESR, and 2 smooths elsewhere) offers a substantial improvement over the use of 3 pre- and post-CGC smooths over the whole domain. We see that at high resolutions (level = 9 through 11) the error begins to rise again. To obtain results in keeping with second order convergence at resolutions up to level = 11, more work is required. The use of 3 pre- and post-CGC smooths *with* the ESR (i.e., 6 smooths in the ESR, and 3 elsewhere) produces results comparable to those obtained by using 6 pre- and post-CGC smooths over the whole domain, however the former requires a fraction of the computational cost of the latter.

that the former case (pre-CGC) would require at least as much smoothing as the latter (post-CGC); we see evidence for this in the two-hole solutions, such as those used to produce Figure 5. Again we are able to achieve second order convergence, for instance with 1 V-cycle, 12 pre-CGC sweeps and no post-CGC sweeps, and with more effort: 5 V-cycles, 20 pre- and post-CGC sweeps, shown for comparison as a “perfect” multigrid result.

### 3.2. Three dimensions

For solving equations in 3D, we proceeded by steps, performing a few test cases until arriving at a code which solves an equation which is similar to the Hamiltonian constraint in 3+1 general relativity.

The first test case is similar to the 2D case discussed above, i.e., we choose  $f(x, y, z)$  such that the exact solution to (21) is

$$u(x, y, z) = \sin(\pi l_x x) \sin(\pi l_y y) \sin(\pi l_z z) \quad (27)$$

where  $l_x$ ,  $l_y$  and  $l_z$  are integers which we set to unity. We excised a sphere of radius  $r_{\text{mask}} = 0.129$ , which is a value chosen simply to ensure that the size of the mask is different on different grid levels, i.e. to make the test a bit more difficult than if we

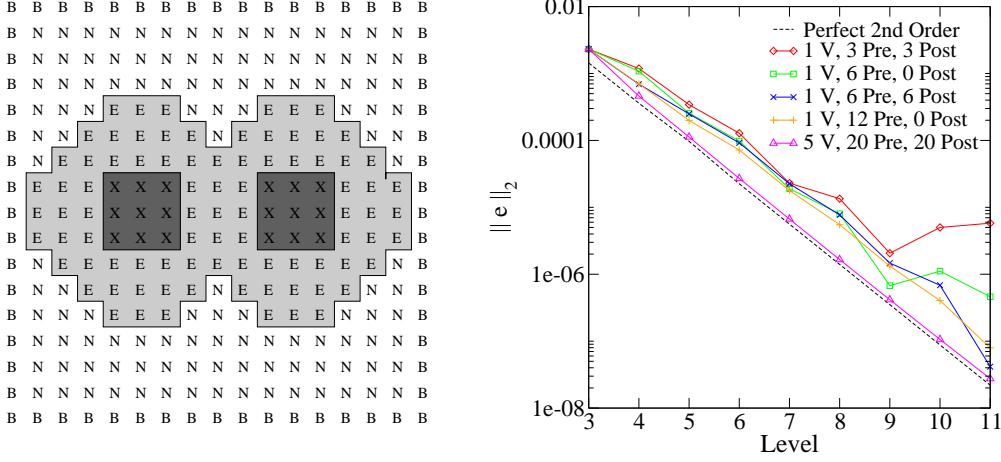


**Figure 5.** Comparison of pre-CGC smoothing vs. post-CGC smoothing, for a domain with two circular holes of radius  $r_{\text{mask}}=0.1$ , separated by a distance  $d = 0.2$ , again for Eqs. (22)-(25). Since a pre-CGC smooth requires the same number of operations as a post-CGC smooth, runs with 1 V-cycle, 3 pre- and 3 post-CGC smooths are as costly as runs with 1 V-cycle, 6 pre- and 0 post-CGC smooths. However the latter parameters yield a somewhat lower error at all resolutions. In another case, we compare 6 pre- and 6-post CGC smooths with 12 pre- and 0 post-CGC smooths, with the similar result that 12 pre- and 0 post-CGC smooths yield lower error. We note that the general shapes of these graphs seem to alternate between ‘turning down’ and ‘turning up’, with the cases involving more computational cost producing results closer to the ideal line. This suggests that, for a given range of resolutions, one is able to obtain results closer and closer to second order convergence as one increases the computational cost; an ‘extreme’ case of 5 V-cycles, with 20 pre- and 20 post-CGC smooths is shown to illustrate this. It is important to note that post-CGC smoothing is not negligible in all cases: One needs post-CGC smooths particularly for runs involving multiple V-cycles in order to ensure convergence, e.g., a 3 V-cycle run with 12 pre- and 0 post-CGC smooths *immediately* begins to ‘blow up’ as the resolution is increased. Adding post-CGC smooths to such a run considerably improves the convergence.

had chosen some multiple of the mesh spacing. For the test case involving a sinusoidal solution (27), the results are very similar to those of the 2D case. Having verified that the multigrid solver could adequately handle such a system and achieve second order accuracy, we proceeded to the next step.

The next test case involves an equation (20) which corresponds to the solution of Hamiltonian constraint equation for conformally flat spacetimes system[37]:

$$\nabla^2 u - K^2 u^5 + \frac{A^2}{u^7} = f, \quad (28)$$

where  $K^2$  and  $A^2$  are arbitrary positive real constants related to the expansion rate of the 3-space, and  $r$  is the usual radial coordinate. We adjust the matter source term  $f(x, y, z)$  such that the continuum solution is

$$u(x, y, z) = 1 + 2M/r. \quad (29)$$

Here  $r$  is the usual radial coordinate, and we choose  $M = 1$ . The excision region contains  $r = 0$  and the function values in this region are not calculated. On the inner boundary (the boundary of the excision region), we use values of the continuum

solution as Dirichlet conditions on *only the finest grid*, and on coarser grids, we use data copied or extrapolated from finer grid data. One can simply copy values from the fine grid to the coarse grid wherever the boundary points on the fine and coarse grids coincide. Wherever they do not coincide, i.e., wherever the coarse grid boundary points are ‘interior’ to the fine grid boundary points, we find it quite adequate to use quadratic extrapolation (in one dimension) from the neighboring (non-excised) fine grid points to obtain the value at the location of a coarse grid boundary point. The results we obtain appear to be rather insensitive to the form of the extrapolation used (e.g., the shape of the stencil). The use of extrapolated fine-grid data is an important difference from the way inner boundary values are obtained in the 2D code, and does constitute a great improvement over the generic applicability of our method.

For the outer boundary in this case, we can either apply Dirichlet conditions using the continuum solution  $u(x, y, z)$ , or we can use a mixed boundary condition called the *Robin* condition. The Robin condition requires

$$\frac{\partial}{\partial r}[r(u - 1)] = 0, \quad (30)$$

on the boundary. The Robin condition is the standard condition used in relativity when a solution with the form (29) is desired (see, e.g., [37]). However  $M$  is not a known constant until the solution is known, so the condition which the solution (29) satisfies, namely (30), is implemented as the boundary condition.

There are several ways to implement the Robin condition. Rather than taking derivatives in the radial direction as required by (30), we follow Alcubierre [38] and instead take derivatives only in directions normal to the faces of our cubical domain. This approach is much simpler to implement than using radial derivatives. We implement this using first order difference stencils; for the  $+x$  face of the domain, at location  $x_i$ , the stencil is simply

$$\tilde{u}_{i,j,k} = 1 + (\tilde{u}_{i-1,j,k} - 1) \frac{r_{i-1,j,k}}{r_{i,j,k}}, \quad (31)$$

where  $r_{i,j,k}$  is the radial distance to lattice location  $(i, j, k)$ . We have also implemented alternative stencils: second order stencils in the normal direction, and a first order stencil in the radial direction.

### Smoothing Operations

We use a simple “red-black” Gauss-Seidel Newton iteration to smooth the error, i.e.,

$$\begin{aligned} r_{GS} = h^{-2} & (\tilde{u}_{i+1,j,k} + \tilde{u}_{i-1,j,k} + \tilde{u}_{i,j+1,k} + \tilde{u}_{i,j-1,k} \\ & + \tilde{u}_{i,j,k+1} + \tilde{u}_{i,j,k-1} - 6\tilde{u}_{i,j,k}) \\ & - K^2 \tilde{u}_{i,j,k}^5 + A^2 \tilde{u}_{i,j,k}^{-7} - f_{i,j,k} \end{aligned} \quad (32)$$

$$\tilde{u}_{i,j,k} = \tilde{u}_{i,j,k} - \frac{r_{GS}}{-5K^2 \tilde{u}_{i,j,k}^4 - 7A^2 \tilde{u}_{i,j,k}^{-8} - 6h^{-2}} \quad (33)$$

### Restriction and Prolongation Operators

For the restriction operator  $I_h^{2h}$ , we use a weighted average which is defined via a  $3 \times 3 \times 3$  stencil, with a weight of  $1/8$  on the central point,  $1/16$  on the center of

each face,  $1/32$  on the center of each edge and  $1/64$  on each corner, i.e.: [30]

$$\begin{aligned}
 \tilde{u}_{I,J,K}^{2h} = I_h^{2h} \tilde{u}^h = & \frac{1}{8} [\tilde{u}_{i,j,k}^h \\
 & + \frac{1}{2} (\tilde{u}_{i+1,j,k}^h + \tilde{u}_{i-1,j,k}^h + \tilde{u}_{i,j+1,k}^h \\
 & \quad + \tilde{u}_{i,j-1,k}^h + \tilde{u}_{i,j,k+1}^h + \tilde{u}_{i,j,k-1}^h) \\
 & + \frac{1}{4} (\tilde{u}_{i,j+1,k+1}^h + \tilde{u}_{i,j-1,k+1}^h + \tilde{u}_{i,j+1,k-1}^h + \tilde{u}_{i,j-1,k-1}^h \\
 & \quad + \tilde{u}_{i+1,j,k+1}^h + \tilde{u}_{i-1,j,k+1}^h + \tilde{u}_{i+1,j,k-1}^h + \tilde{u}_{i-1,j,k-1}^h \\
 & \quad + \tilde{u}_{i+1,j+1,k}^h + \tilde{u}_{i-1,j+1,k}^h + \tilde{u}_{i+1,j-1,k}^h + \tilde{u}_{i-1,j-1,k}^h) \\
 & + \frac{1}{8} (\tilde{u}_{i+1,j+1,k+1}^h + \tilde{u}_{i-1,j+1,k+1}^h + \tilde{u}_{i+1,j-1,k+1}^h \\
 & \quad + \tilde{u}_{i-1,j-1,k+1}^h + \tilde{u}_{i+1,j+1,k-1}^h + \tilde{u}_{i-1,j+1,k-1}^h \\
 & \quad + \tilde{u}_{i+1,j-1,k-1}^h + \tilde{u}_{i-1,j-1,k-1}^h)] \quad (34)
 \end{aligned}$$

As in the 2D case, if any of the fine grid points included in the weighting are inner boundary points, then we use a simple copy instead of weighted restriction

For the prolongation operator  $I_{2h}^h$ , we use simple trilinear interpolation.

### 3.3. 3D Results

A graph of the convergence behavior for the solution of the conformally flat background Hamiltonian constraint, Eq. (28), is given in Figure 6. The left panel shows that we obtain lines which run parallel to the line for second order behavior at high resolutions, for both a Dirichlet outer boundary condition and the “first order perpendicular” implementation of the Robin condition suggested by Alcubierre [38]. In fact, the two graphs we obtain lie on top of each other. The right panel shows the convergent solution error of our solutions (i.e. the difference between our solutions and the exact, continuum solution)

## 4. Toward More General Applications

We have made use of a known exact solution in two key elements of this paper: (1) supplying values for Dirichlet conditions on the inner boundary, and (2) calculating the solution error  $e \equiv u - \tilde{u}^h$  for measuring the accuracy and convergence of the code. Since we wish to use the multigrid solver for situations in which an exact solution is not known across the whole domain (such as in a solution for the conformal factor in a general binary black hole spacetime), we describe here the modifications to the previous discussion in the absence of an exact solution.

In the 2D code we used the continuum solution to supply Dirichlet conditions on the inner boundaries of all multigrid levels, however for the 3D code we only used the continuum solution on the finest grid, and then extrapolated or copied data from finer grids to coarser grids. (There was nothing about the 2D case that made extrapolation impossible; rather it was simply a later feature which was added to the more advanced 3D code.) Although we were able to employ this extrapolation effectively in the cases we tried — using a very simple, almost arbitrary, 1D extrapolation method — it may be that such a method would be unstable for certain classes of equations. Although we see no evidence for this, and given the generality of the multigrid method one may expect much of what is found in this paper to apply to other systems of interest. We cannot offer complete assurance that extrapolation will work for all elliptic systems.

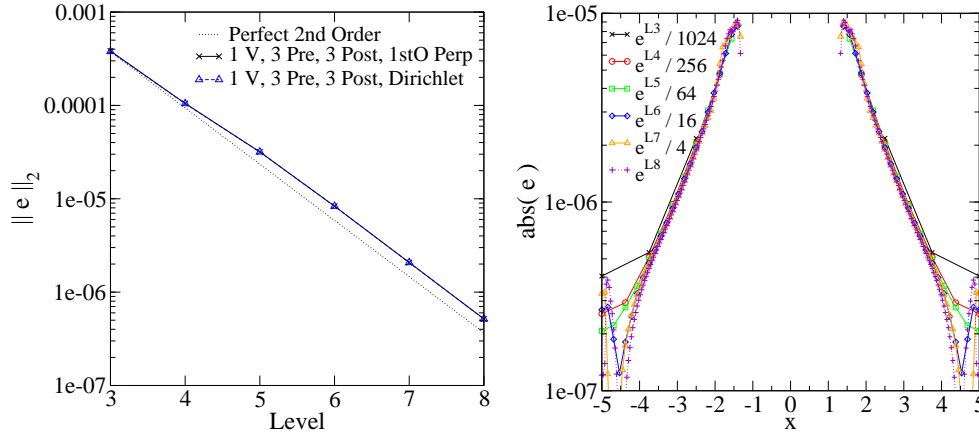


**Figure 6.** Convergence results for 3D solutions to (28) of the form  $u = 1 + 2M/r$ , for runs in which  $A^2 = K^2 = 1$ ,  $l_{\min} = 3$ , and  $r_{\text{mask}} = 1.29$ , for a domain  $[-5, -5, -5]$  to  $[5, 5, 5]$ . Left panel: A logarithmic plot of the L2 norm of the solution error  $e = u - \tilde{u}^h$ , showing a comparison between outer boundary conditions. Using the “first order perpendicular” (FOP) implementation (31) of the Robin boundary condition (30)), we obtain convergence results which lie on top of those obtained using a Dirichlet outer boundary condition (where the values of the continuum solution are supplied at the outer boundary). These results also run parallel to the line for perfect second order behavior. Right Panel: A logarithmic plot of  $e$  itself, at the end of each V-cycle in the Full Multigrid Algorithm. These results correspond to the “1V, 3 Pre, 3 Post, 1st order Perp” case shown in the left panel. Here we show a 1D slice along the x-axis, and we have divided coarser grid values by appropriate powers of four in order to make the comparison. We see second order convergence over the interior of the domain and, importantly, in the vicinity of the excision region. Near the outer boundary, the magnitude of the error is roughly second order (thus it does not noticeably affect the graph shown in the left panel), however its shape is resolution-dependent. This feature may arise from the use of the FOP condition.

The assumption that an exact value is known at points on the finest grid may not be appropriate for many of the solutions of interest to numerical relativists. One may encounter systems with Neumann or Robin conditions at the inner boundary. Although we have not considered such cases explicitly, we suggest straightforward differencing similar to the treatment of the Robin conditions we reported above.

When one cannot measure the accuracy of the code by calculating the solution error, one can still gain a measure of the convergence of the code by monitoring the relative truncation error  $\tau_h^{2h}$ . One should disregard values at points adjacent to inner boundary points, as these tend to be poorly defined and exhibit blow-up behavior, but all other points are eligible for comparison. A plot of  $\tau_h^{2h}$  at various grid levels for a 3D solution is shown in Figure 7, demonstrating the strict second order behaviour of the solution on two different domains.

## 5. Conclusions

We can offer five tips for those who wish to implement 2D or 3D multigrid methods for domains with holes.

- 1) The first and most important tip is really twofold:

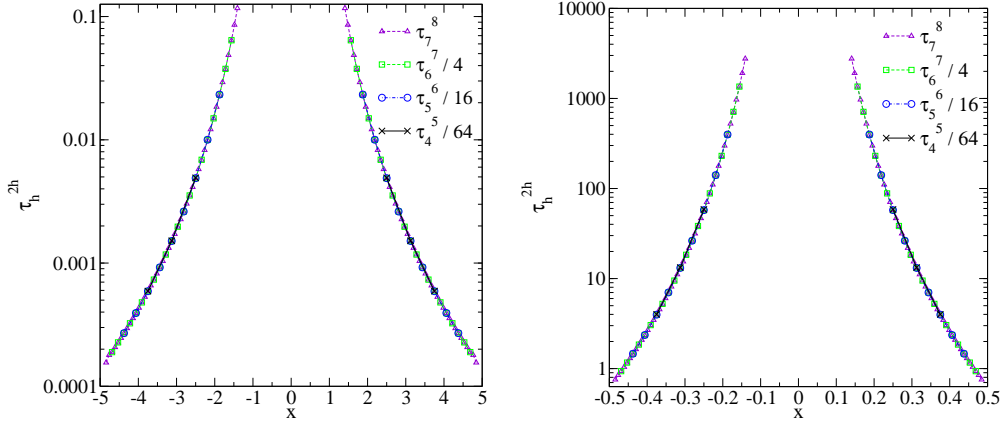


**Figure 7.** A 1D slice through the center of a 3D domain, for the truncation error of a solution to Eq. (28) with Robin outer boundary conditions, seeking a solution of the form  $u = 1 + 2M/r$ . The run parameters  $K^2$ ,  $A^2$  and  $M$  are set to unity, and we perform 1 V-cycle, 3 pre-CGC smooths and 3 post-CGC smooths. Left panel: On the domain  $[-5, -5, -5]$  to  $[5, 5, 5]$ , with  $r_{mask} = 1.29$ . Right panel: On the domain  $[-0.5, -0.5, -0.5]$  to  $[0.5, 0.5, 0.5]$ , with  $r_{mask} = 0.129$ . (This smaller domain is intended to provide a stronger test of the algorithm than the larger domain.) The notation  $\tau_x^y$  in the figure legends denotes which grid levels were used to calculate  $\tau_h^{2h}$  for a given set of points. We see that, on both domains, the  $\mathcal{O}(h^2)$  error function is independent of resolution, in accordance with the idea of Richardson extrapolation. Since the continuum solution is  $u(x, y, z) = 1 + 2M/r$ , we expect the error function to tend toward large values as  $r \rightarrow 0$ . In these graphs, we have cut out the values of  $\tau_h^{2h}$  immediately adjacent to the inner boundary.

- apply inner boundary conditions on points immediately *interior to* (rather than exterior to, as is often done) some spatial surface such as a circle or sphere of a given radius. This has the effect that the extent of excision region is smaller on coarser grids than on finer grids.
- when performing restriction operations, use weighted restrictions on all interior points, *except* in cases where the weighted operator would include points where the inner boundary conditions are applied. For these latter cases, use a simple copy operation.
- 2) Concentrate smoothing operations where they are most needed. We have done this by arbitrarily defining an “extra smoothing region” around any hole, and performing twice as many smooths in this region as in the rest of the domain. One can imagine more sophisticated schemes, which look at derivatives of the solution or the local truncation error as indicators of where the extra smoothing should be performed and how much extra work should be performed there.
- 3) It may be the case that pre-CGC smoothing is much more effective than post-CGC smoothing for a given problem, particularly if only one V-cycle is performed. Concentrating the bulk of the smoothing operations into the pre-CGC smooths results in a faster route to the solution at a desired accuracy.
- 4) This repeats the advice of Alcubierre [38] (Radial) Robin boundary conditions can be adequately mimicked by applying them only in the normal directions, thus simplifying the computer code and reducing the computation effort slightly. The Robin conditions should be applied at all grid levels; i.e. it is *not* the case that



one should apply Robin conditions on the finest grid only and then use those values as Dirichlet conditions on coarser grids.

- 5) This tip is intended for use in situations where an exact solution is not available; we have less experience with these situations. However, we find that a naive quadratic extrapolation from nearby points is adequate to provide values for Dirichlet boundary conditions on the edge of the hole. Further (more technically), when monitoring the relative truncation error  $\tau_h^{2h}$ , points immediately adjacent to inner boundary points have erratic behavior, and should not be considered in judging the behavior of the solution.

We clearly have some further work ahead in order to consider more general systems in which our inner boundary data is not so easily obtained, and we also need to consider systems more complex than the Hamiltonian constraint for a conformally flat background, as treated in this paper. It is thus our hope that the techniques described here will also be of relevance for more interesting systems of elliptic equations. We are developing a solver for the full set of constraint equations (testing it using the Kerr-Schild-type binary black hole data described in [39]), and see promising results using precisely the techniques given in this paper. Further improvements in the speed of multigrid scheme, such as the use parallelism and adaptivity [40, 41, 42] will also likely be necessary for its practical application in a constrained evolution code.

The 2D and 3D codes described here are available for use by the community, by download from [http://wwwrel.ph.utexas.edu/~shawley/mg\\_ex.html](http://wwwrel.ph.utexas.edu/~shawley/mg_ex.html). We encourage other users of our approach. However, the codes are “as is”, and we cannot maintain them, nor correct problems that may arise from their use.

## 6. Acknowledgments

We thank Matthew Choptuik for helpful discussions, and for the use of his notes and his 2D FAS multigrid code. We also thank Miguel Alcubierre, Bernd Brügmann, Gregory Cook, Lee Lindblom, Mark Scheel, Frans Pretorius, James Isenberg and Sergio Dain for helpful discussions. We thank Jonathan Thornburg and Ian Hawke for their helpful comments on a previous draft of this paper, and we thank Roberto Gomez for pointing out the Udaykumar et al. reference [29] to us. This work was supported by NSF grant PHY 0102204. Portions of this work were conducted as part of the Caltech Visitors Program on the Initial Data Problem, and at the Kavli Institute for Theoretical Physics, The University of California at Santa Barbara, under NSF grant PHY 9907947.

- [1] Arnowitt R, Deser S, Misner C W 1962 in *Gravitation: An Introduction to Current Research*, L. Witten ed. Wiley
- [2] York J W 1979 in *Sources of Gravitational Radiation*, L. Smarr ed., Cambridge University Press.
- [3] Siebel F and Hübner P 2001 *Phys. Rev.* **D64** 024021
- [4] Calabrese G, Pullin J, Sarbach O, Tiglio M, and Reula O 2002 *gr-qc/0209017*
- [5] Tiglio M 2003 *gr-qc/0304062*
- [6] Yoneda G and Shinkai H 2003 *Class. Quant. Grav.* **20** L31
- [7] Alcubierre M, Allen G, Bona C, Fiske F, Goodale T, Guzman F S, Hawke I, Hawley S H, Husa S, Koppitz M, Lechner C, Pollney D, Rideout D, Salgado M, Schnetter E, Seidel E, Shinkai H, Shoemaker D, Szilágyi B, Takahashi R and Winicour J 2003 *gr-qc/0305023*
- [8] Abrahams A A and Evans C R 1993 *Phys. Rev. Lett.* **70** 2980
- [9] Choptuik M W, Hirschmann E W, Liebling S L, and Pretorius F 2003 *Class. Quant. Grav.* **20** 1857

- [10] Choptuik M W, Hirschmann E W, Liebling S L, and Pretorius F 2003 **gr-qc/0305003**
- [11] Schnetter E 2003 Ph.D. dissertation, University of Tübingen. In preparation.
- [12] Meier D L 2003 In preparation
- [13] Anderson M and Matzner R A 2003 **gr-qc/0307055**.
- [14] Brandt A 1977 *Math. of Computation* **31** 333
- [15] Kidder L E and Finn L S 2000 *Phys. Rev.* **D62** 084026
- [16] Pfeiffer H P, Kidder L E, Scheel M A and Teukolsky S A 2003 *Comput. Phys. Commun.* **152** 253
- [17] Klasky S 1994 Ph.D. dissertation, University of Texas at Austin
- [18] Choptuik M W 2002 Personal communication, Dec. 2
- [19] Choquet-Bruhat Y, Isenberg J and York, J W 2000 *Phys. Rev.* **D61** 084034
- [20] Dain S 2001 *Phys.Rev.* **D64**, 124002.
- [21] Maxwell D 2003, **gr-qc/0307117**.
- [22] Brandt A 1982 in *Lecture Notes in Mathematics* **960** (Multigrid Methods) W. Hackbusch and U. Trottenburg, eds, Academic Press, New York/London, 53-147.
- [23] Hackbusch W 1985 *Multi-Grid Methods and Applications*, Springer Series in Comp. Math. 4, Springer Verlag
- [24] Stüben K and Trottenburg U 1982 in *Multigrid Methods: Proceedings of Köln-Porz, 1981*, W. Hackbusch and U. Trottenburg, eds, Springer-Verlag Berlin
- [25] Wesseling P 1980 in *Numerical Analysis. Proceedings, Dundee 1979* G.A. Watson, ed., *Lecture Notes in Mathematics* **773** Springer-Verlag, Berlin 164
- [26] Wesseling P 1992 *An Introduction to Multigrid Methods*, Wiley, Chichester (Available online at <http://www.mgnet.org/mgnet-books-wesseling.html>)
- [27] Briggs W L, Henson V E and McCormick S F 2000 *A Multigrid Tutorial*, 2nd ed.
- [28] Johansen H and Colella P 1998 *J. Comp. Phys.* **147** 60.
- [29] Udaykumar H S, Mittal R, Rampunggoon P and Khanna A 2001 *J. Comp. Phys.* **174** 345.
- [30] Brandt S and Brüggmann B 1997 *Phys. Rev. Lett.* **78**. See also Brüggmann B 1998 in *Eighteenth Texas Symposium on Relativistic Astrophysics and Cosmology, Chicago, 1996*, eds. A. Olinto, J. Frieman, and D. Schramm, World Scientific Publishing, Singapore
- [31] Press W H, Teukolsky S A, Vetterling W T and Flannery B P 2001 *Numerical Recipes in Fortran 77, 2nd ed.*, Cambridge University Press, 862
- [32] Choptuik M W 1999 Lecture notes, Taller de Verano 1999 de FENOMECC: Numerical Analysis with applications in Theoretical Physics.
- [33] Choptuik M W and Unruh W G 1986 *Gen. Rel. Grav.* **18** 813
- [34] Brandt A 1988 *Class. Quantum Grav.* **5** 713
- [35] Choptuik M W 1998 **mgfas2d**, in lecture notes for Physics 381C - Computational Physics, University of Texas at Austin
- [36] Pretorius F 2002 Ph.D. dissertation, University of British Columbia, 42-43.
- [37] York J.W. and Piran T. 1982 in: *Spacetime and Geometry*, eds. R. Matzner, L. Shepley, University of Texas Press, Austin, 145.
- [38] Alcubierre M 2003 Personal communication, Feb. 18
- [39] Bonning E, Marronetti P, Neilsen D and Matzner R A 2003 *Phys. Rev.* **D68**, 044019.
- [40] Griebel M and Zumbusch G 1998 in Proceedings of ParCo '97, E. D'Hollander, G.R. Joubert, F.J. Peters, U. Trottenburg, eds., Elsevier, 589-599.
- [41] Brown D and Lowe L 2003 Penn State Numerical Relativity Lunch Talk, February 21, [http://www.astro.psu.edu/nr/nrlunch/2003/2003\\_02\\_21\\_Brown/Transparencies.pdf](http://www.astro.psu.edu/nr/nrlunch/2003/2003_02_21_Brown/Transparencies.pdf).
- [42] Baker B 2002 Ph.D. dissertation, University of Florida, 57